TITLE:

One-dimensional imidazole aggregate in aluminium porous coordination polymers with high proton conductivity

AUTHOR(S):

Bureekaew, Sareeya; Horike, Satoshi; Higuchi, Masakazu; Mizuno, Motohiro; Kawamura, Takashi; Tanaka, Daisuke; Yanai, Nobuhiro; Kitagawa, Susumu

京都大学
KYOTO UNIVERSITY

KURENAI 紅
Kyoto University Research Information Repository

1

One-Dimensional Imidazole Aggregate in Aluminum Porous Coordination Polymers with High Proton Conductivity

Sareeya Bureekaew[1,5], Satoshi Horike[1,5], Masakazu Higuchi[2], Motohiro Mizuno[3], Takashi Kawamura[1],

Daisuke Tanaka[1], Nobuhiro Yanai[1], Susumu Kitagawa[1,4,5]

(1) Department of Synthetic Chemistry and Biological Chemistry, Graduate School of Engineering, Kyoto University,

Katsura, Nishikyo-ku, Kyoto 615-8510, Japan,

(2) RIKEN, SPring-8 center, 1-1-1, Kouto, Sayo-cho, Sayo-gun, Hyogo 679-5148, Japan

(3) Department of Chemistry, Graduate School of Natural Science and Technology, Kanazawa University, Kanazawa

920-1192, Japan

(4) Institute for Integrated Cell-Material Sciences (iCeMS) Kyoto University, Yoshida, Sakyo-ku, Kyoto 606-850,

Japan,

(5) Kitagawa Integrated Pore Project, Exploratory Research for Advanced Technology (ERATO), Japan Science and

Technology Agency (JST), Kyoto Research Park, 134 Chudoji Minami-machi, Shimogyo-ku, Kyoto 600-8813, Japan

CORRESPONDING AUTHOR FOOTNOTE

    Dr. Susumu Kitagawa

    Department of Synthetic Chemistry and Biological Chemistry,

    Graduate School of Engineering, Kyoto University

    Katsura, Nishikyo-ku, Kyoto 615-8510, Japan

    TEL: +81-75-383-2833

    FAX: +81-75-383-2732

    e-mail: kitagawa@sbchem.kyoto-u.ac.jp

1 ABSTRACT: *The development of anhydrous proton-conductive materials operating at temperatures*

2 *above 80 ℃ is a challenge that needs to be met for practical applications. Herein, we propose the new*

3 *idea of encapsulation of a proton-carrier molecule—imidazole in this work—in aluminum porous*

4 *coordination polymers for the creation of a hybridized proton conductor under anhydrous conditions.*

5 *Tuning of the host–guest interaction can generate a good proton-conducting path at temperatures above*

6 *100 ℃. The dynamics of the adsorbed imidazole strongly affect the conductivity determined by ^2H*

7 *solid-state NMR. Isotope measurements of conductivity using imidazole-d₄ showed that the*

8 *proton-hopping mechanism was dominant for the conducting path. This work suggests that the*

9 *combination of guest molecule and a variety of microporous frameworks would afford highly mobile*

10 *proton carriers in solids and gives an idea for designing a new type of proton conductor, particularly*

11 *for high temperature and anhydrous conditions.*

12

15

16   Anhydrous proton−conducting solids that are able to operate at high temperature (~120 °C) are

17 required in fuel cell technology.[1,2] Heterocyclic organic molecules such as imidazole or benzyl

18 imidazole have attracted considerable attention for this purpose because they are nonvolatile molecules

19 with high boiling points, and they can exist in two tautomeric forms with respect to a proton that moves

20 between the two nitrogen atoms, which supports a proton transport pathway.[3,4] The protonic defect may

21 cause local disorder by forming protonated and unprotonated imidazoles. In such materials the proton

22 transport may occur through structure diffusion which involves proton transfer between the imidazole

23 and the imidazolium ion through the hydrogen−bonded chain, including the molecular reorientation

24 process for subsequent intermolecular proton transfer.[1] Theoretically, the magnitude of the ionic

25 conductivity is given as

$$\sigma(T) = \sum n_i q_i \mu_i \qquad\qquad (1)$$

where n_i is the number of carriers, and q_i and μ_i are the charge and mobility of the carriers, respectively.[5] Both a large amount and a high mobility of ion carriers are required to provide good proton conductivity. Hence it is important to find suitable materials that meet these requirements. For instance, solid imidazole has a low conductivity ($\sim 10^{-8}$ S cm^{-1}) at ambient temperature[6] although the imidazole density (n_i) is adequately high. This is because the dense packing of imidazole, with strong hydrogen bonding in the solid state, decreases the mobility of each molecule (μ_i).

The main goal of proton conductor modification should therefore be an improvement of the mobility of proton carriers. It is known that local and translational motion of proton carriers strongly affect the proton transfer rate.[1] In order to control the mobility of proton carriers, additional support matrices such as flexible organic polymers or high-porosity solids that afford movable space for a carrier are considered promising.

Porous coordination polymers (PCPs) or metal organic frameworks constructed from transition metal ions and organic ligands have received much attention over the past few years because of their promising applications, such as in gas storage,[7-11] separation,[12-17] catalysis,[18-26] and conductivity.[27-29] Recent developments in approaches to combine PCP frameworks and functional guests such as polymers,[30,31] metals,[22,32-34] or small organic molecules[35-37] on a molecular scale have prompted us to create hybrid materials with novel performance based on the feature that crystalline nanochannels can afford a unique assembly field for functional guests with specific host–guest interactions. The guests in the nanospace of PCPs exhibit unusual behavior compared to in the bulk phase because each manner of assembly is heavily dependent on the nature of the PCP channels, such as their size, shape and chemical environment. Hence, we propose the use of PCPs for incorporation with proton carrier molecules because they can contribute to provide desirable working space for carrier molecules, with high mobility, and show an appropriate packing structure, for improved proton conductivities at high temperatures and under anhydrous conditions (Figure 1).

1   In this study we focused on two types of PCPs with 1D channels and high thermal stability (~400

2   °C), and imidazole as the guest proton carrier molecule. Taking the size and shape of imidazole (4.3 ×

3   3.7 Å^2) into consideration, we chose to use the aluminum compounds [Al(μ_2-OH)(1,4-ndc)]$_n$ (**1**; 1,4-ndc

4   =   1,4-naphthalenedicarboxylate)[38]   and   [Al(μ_2-OH)(1,4-bdc)]$_n$ (**2**;   1,4-bdc   =

5   1,4-benzenedicarboxylate),[9,39] both of which have pore dimensions of ca. 8 Å, but different pore shapes

6   and surface potential, and installed imidazole in each host material. We found that the nanochannels

7   potentiated the different packing of imidazole, compared with the bulk solid imidazole. Conductivity

8   measurements for each of the PCP–imidazole composites at various temperatures and under anhydrous

9   condition presented different profiles because of the different characteristics of the channels of the

10   respective PCPs, resulting in different host–guest interactions, and **1**⊃Im had a conductivity of 2.2 ×

11   10^{-5} S cm^{-1} at 120 °C. We investigated the behavior of absorbed imidazole in the micropores by means

12   of the solid-state NMR technique, and succeeded in determining a good correlation between the features

13   of the host channels, guest mobility and proton conductivity.

14   **Structural information of 1 and 2**

15   The structures of **1** and **2** comprise an infinite number of chains of corner–sharing AlO$_4$(μ_2-OH)$_2$

16   interconnected by the dicarboxylate ligand, resulting in a 3D framework containing 1D channels. The

17   guest–free structures of **1** and **2** are shown in Figure 2. Crystallographic structures show that the pore

18   surfaces of **1** and **2** are composed of hydrophobic (aromatic naphthalene and benzene ring) and

19   hydrophilic (AlO$_4$(μ_2-OH)$_2$) parts. The principal difference between the two aluminum frameworks

20   arises from the difference in ligands 1,4-ndc and 1,4-bdc. Because of asymmetric bridging ligand, **1**

21   consists of two kinds of rectangular channels with dimensions of 7.7 × 7.7 Å^2 and 3.0 × 3.0 Å^2 running

22   along the *c* axis (Figure 2a). This compound shows the property of a rigid framework. Figure 2b shows

23   that steric hindrance arising from the bulky naphthalene ring of the 1,4-ndc ligand of **1** induces

24   restriction of interaction between the polar guest molecule and μ_2-OH and/or carboxylate group of the

25   framework. Because of the absence of an accessible hydrophilic pore surface the hydrophobic character

1   from the aromatic part of the naphthalene ring of the ligand is dominant. In other words, **1** provides two

2   types of microchannels with hydrophobic pore surfaces.

3   In the case of **2** the framework exhibits only 1D diamond−shaped channels composed of the smaller

4   benzene moieties of 1,4-bdc, with dimensions 8.5×8.5 Å^2, running along the *a* axis. Eventually, the

5   polar sites on the surface are exposed to guest molecules, which enhances guest−induced structural

6   transformation of **2,** with the aid of the interaction between the imidazoles and μ_2-OH and/or a

7   carboxylate groups.[40] Thus, it is intriguing that a simple modification on the organic moiety produces

8   channels with different nature, hydrophobic and hydrophilic for **1** and **2,** respectively. [39]

9   **Properties of the inclusion compounds**

10   The thermogravimetric (TG) profiles of **1**⊃Im and **2**⊃Im are shown in Figure 3. Note that**1**⊃Im and

11   **2**⊃Im indicate the imidazole hybrid compound of **1** and **2**, respectively. The existence of imidazole in **1**

12   and **2,** without any reactions/conversion, was confirmed by thermogravimetry/mass spectrometry

13   (TG–MS). The TG profile of **1**⊃Im shows 14% weight imidazole loading or 0.6 imidazole/1 Al ion. The

14   release of accommodated imidazole commences at 160 °C and completes at 225 °C. In the case of **2,** the

15   loaded imidazole amounts to 30% weight or 1.3 imidazole/1 Al ion, which is twice as much as in **1**. The

16   TG curve shows that the loss of imidazole molecules in **2**⊃Im occurs in two steps: in the first step, the

17   release of imidazole commences at 130 °C and is completed by approximately 160 °C and in the second

18   step it commences at 160 °C and is completed by 240 °C. The percentage imidazole loss is half the

19   amount of the imidazole, followed by the residual in the second step.

20   The one single step mass loss in **1**⊃Im is indicative of uniformly accommodated imidazole

21   molecules. On the other hand, based on the TG curve of **2**⊃Im, there are two types of imidazole

22   molecules installed in the channel. According to the amphiphilic nature of the surface of the channel, the

23   imidazoles with strong interaction with the hydrophilic sites of a μ_2-OH or a carboxylate group are

24   released at higher temperature (160 – 240 °C), correlated to the weight loss in second step, whereas the

25   imidazoles which have less interaction with pore surface are removed in the first step (below 160 °C).

1   The crystal structures of **1** and **2** (Figure 2) reveal the following. Compound **1** consists of two types

2   of 1D channels, namely small channels with dimensions 3.0×3.0 Å^2 in which imidazole is unable to be

3   installed: only large channels with dimensions of 7.7×7.7 Å^2 can install the guest. Compared with

4   **2**⊃Im, half the amount of accommodating imidazole per one Al is reasonable from crystal structures.

5   Considering that the dispersion of imidazole is uniform in the crystalline channel we could calculate

6   the density of imidazole in the larger channels of **1** (443 Å^3) and channels of **2** (750 Å^3). This was

7   calculated from the void space of the guest−free state by using the PLATON software package.[41] The

8   values were about 0.15 and 0.19 g cm^{-3}, respectively. However, as the structure of **2** changes after

9   accommodation of imidazole and it is difficult to determine the density of imidazole in **2**⊃Im. The

10   density of imidazoles in **1**⊃Im and **2**⊃Im are much smaller than that of solid bulk imidazole, which is

11   1.23 g cm^{-3} at ambient temperature.[42] This evidence indicates that the behaviors of imidazoles loaded to

12   the framework considerably differ from bulk imidazole resulting from the space effect.

13   The X−ray powder diffraction (XRPD) patterns shown in Figure 4 show that the diffraction pattern

14   of **1**⊃Im is the same as that of apohost **1**, corresponding to the robustness of **1**. Conversely, the peak

15   positions and pattern of **2**⊃Im are different from those of apohost **2** and the shrinkage after installation

16   of imidazole is observed. This is because of strong interaction between the polar imidazole and

17   hydrophilic pore surface of flexible **2**.

18   **Conductivity of 1⊃Im and 2⊃Im**

19   We aimed to achieve proton conductivity at temperatures around 100 °C, and hence to design

20   composites that are stable at the target temperatures. We already confirmed that the prepared composites

21   **1**⊃Im and **2**⊃Im are stable up to 130 °C without any loss from TG. Conductivities of **1**⊃Im and **2**⊃Im

22   were measured by AC impedance spectroscopy, which is a versatile electrochemical tool to characterize

23   intrinsic electrical properties of materials. Figure 5b and 5c shows Nyquist plots (Z' versus Z'') of the

24   complex impedance measured on **1**⊃Im and **2**⊃Im under a nitrogen atmosphere at 120 °C. The

25   impedance plots of the two complexes are typical of materials with predominant ionic conductivity.

1   They show one semicircle with a characteristic spur at low frequencies, which indicates blocking of H^+

2   ions at the gold electrodes. The magnitude of Z' decreased with an increase in temperature. The

3   conductivity of the samples was calculated from the impedance value using the following equation

4

$$\sigma = \frac{L}{Z \cdot A} \qquad\qquad (2)$$

5   where σ is the conductivity (S cm^{-1}), L is the measured sample thickness (cm), A is the electrode area

6   (cm^2) and Z is the impedance (Ω).

7   The temperature dependence of proton conductivities of **1**, **1**⊃Im and **2**⊃Im, measured under

8   anhydrous conditions at temperatures ranging from 25 to 120 °C, are shown in Figure 5a. Guest−free **1**

9   exhibits a conductivity lower than 10^{-13} S cm^{-1}, confirmed by DC measurement, which is indicative of

10   negligible proton conductivity for this apohost framework. After installation of imidazole the proton

11   conductivity of **1**⊃Im is 5.5×10^{-8} S cm^{-1} at room temperature. Although the mole fraction of imidazole

12   in **1**⊃Im is much smaller than that of bulk imidazole, the proton conductivity of **1**⊃Im is of the same

13   order as that of solid bulk imidazole. This is possibly because of the effect of the nanospace on the

14   dynamic motion of imidazole. The proton conductivity of **1**⊃Im improves significantly as the

15   temperature increases: at 120 °C the proton conductivity reaches 2.2×10^{-5} S cm^{-1}. Note that bulk

16   imidazole at this temperature is no longer in the solid phase. This increase in the temperature dependent

17   conductivity of **1**⊃Im, compared with the conductivity profile of apohost **1**, indicates that a significant

18   improvement in the conductivity arises directly from the accommodated imidazole. Furthermore, the

19   conductivity of **1**⊃Im continuously increases with an increase in temperature with the activation energy

20   of 0.6 eV. This result indicates that phase transition does not take place. The mobile imidazole induces

21   high temperature (> 100 °C) proton conductivity in **1**⊃Im. We can improve the mobility of imidazole by

22   taking advantage of the isolating effect of PCPs. As the evidence from isotope effect (Figure S1), the

23   proton conductivity of our systems is mainly contributed by proton hopping mechanism.

1 In order to improve proton conductivity we increased the amount of loaded imidazole (the number

2 of charge carriers, n_i) by using **2**, which has twice the amount of accessible space for imidazole as the

3 supporting framework. However, the proton conductivity of **2**⊃Im at ambient temperature is about 10^{-10}

4 S cm^{-1}, which is lower than that of **1**⊃Im. As in the case of **1**⊃Im, the conductivity of **2**⊃Im increases as

5 the temperature increases with the activation energy of 0.9 eV, and it reaches 1.0×10^{-7} S cm^{-1} at 120

6 °C. The proton conductivity of **2**⊃Im is about two orders of magnitude lower than that of **1**⊃Im,

7 although the amount of loaded imidazole is higher than that of **1**⊃Im. This is also possibly because of

8 the difference in dynamic motion of the guest, which is based on the interaction between guest and host.

9 Microchannels in compound **1** have nonpolar potential surface and polar imidazole does not interact

10 strongly with the host framework; therefore, it can move freely in this channel. Nonetheless, in the case

11 of polar surface microchannels in **2**, the half amount of imidazole interact strongly with the hydrophilic

12 sites of host framework. The strong host–guest interactions give rise to the shrinkage of the framework,

13 eventually of a unit cell, resulting in the different environment of imidazole accommodated in **2**,

14 compared to in **1**. Therefore, because of strong host–guest interaction and dense packing, the imidazoles

15 with strong interaction with the μ_2-OH and/or carboxylate group of **2** are not allowed to move or rotate

16 freely in the framework. Consequently, the conductivity in **1**⊃Im is larger than in **2**⊃Im.

17 **Direct observation of dynamics of imidazoles in 1⊃Im and in 2⊃Im**

18 Solid-state ^{2}H NMR spectroscopy is suitable for examining the dynamics of target molecules

19 selectively.[43-45] We therefore used this analytical technique to determine the mobility and its correlation

20 with the conductivity of adsorbed imidazole in **1** and **2**. The ^{2}H NMR powder line shapes are sensitive

21 to local molecular motion and are characterized in terms of both the time scale and the mode of the

22 motion, such as rotation or wobbling behavior.[46,47] We introduced imidazole-d_4 for each host instead of

23 nondeuterated imidazole and checked that the adsorbed amount for each guest was identical to that in

24 the normal hosts. The ^{2}H NMR spectra of **1**⊃Im and **2**⊃Im recorded at different temperatures are shown

25 in Figure 6. In the case of **2**⊃Im (Figure 6b), at the lowest measured temperature of 20 °C, we observed

a clear Pake-type doublet pattern with a splitting width of 120 kHz, indicating that the adsorbed

imidazole-d_4 behaves totally anisotropically. As the temperature increases, a narrow Lorentzian-type

peak appears in the middle of the anisotropic powder pattern, corresponding to the emergence of

isotropic imidazole by thermal activation. There are two possible explanations for the spectrum: the first

is that free motional imidazole with low frequency shows a narrow peak and the second is the

simultaneous coexistence of frequencies of slow and fast imidazole. Nonetheless, the spectrum at 40 °C

indicates the existence of activated guests in pores, and the relative intensity of the activated species

increases as the temperature increases to 80 °C.

In the case of **1**⊃Im, spectra also show doublet powder patterns at low temperatures (–20 and –60

°C) with the same splitting width as in **2**⊃Im at temperatures lower than 30 °C. However, a narrow

Lorentzian-type peak starts to appear at 20 °C. This clearly indicates that at ambient temperature the

imidazole in **1** can show isotropic motion with a larger frequency than **2**. The fraction of isotropic

imidazole becomes dominant at 40 °C, and at 80 °C we can no longer observe any Pake-doublet pattern

at all. This suggests that all adsorbed imidazole within the pores of **1** has a fast isotropic motion. Using

the NMR line shapes obtained, we evaluated the motion of the imidazole using a simulation procedure.

We used a free rotation model of imidazole molecules with tetrahedral orientations as the main motion

because this is associated with the Grotthus mechanism. We succeeded in obtaining theoretical patterns

for both samples, at each temperature, based on the tetrahedral free rotational model as shown in Figure

6, and clearly observed that the rotation frequency of **1** is greater than that of **2**. For example, the

frequency of **1** at 60 °C is 45 kHz whereas that of **2** shows 10 kHz, while the frequency of **1** at 20 ℃ (20

kHz) is still larger than that of **2** at 90 ℃ (18 kHz) (see Figure S2). Consequently, we are able to

conclude that the degree of motional behavior of the accommodated imidazole of **1** is greater than in the

case of **2**, which strongly supports the difference in conductivity.

We have presented a new approach to create proton transportation space based on the use of proton

carrier organic molecules to enhance the proton conductivity of solid materials under anhydrous

1   conditions at high temperature. The different values of conductivity of imidazole in compounds **1** and **2**

2   are consistent with the dynamic properties of imidazole adsorbed in the pores. The hydrophilic

3   microporous surface of **2** results in strong interaction with even the half amount the adsorbed imidazoles

4   and significantly decelerates their mobility, resulting in a poor proton transfer rate. On the other hand,

5   because of the hydrophobic and flat pore surface of **1**, adsorbed imidazole can move more freely than in

6   **2** and than bulk phase, and we eventually observe higher proton conductivity, which is comparable to

7   that of a conventional organic polymer conductor such as poly(4-vinylimidazole).[48] PCP can provide an

8   appropriate pore environment and size for target proton carrier by the fine−tuning of their components.

9   In the other word, the optimum mobility and density of proton carriers can be reached by taking

10   advantage of the designability of PCPs. The strategy would be considered significant to prepare hybrid

11   materials high proton−conductive.

12   **Experimental section**

13   **Materials**

14   Aluminium(III) nitrate nanohydrate $Al(NO_3)_3 \cdot 9H_2O$ (WAKO, 99.9%); terephthalic acid

15   $HO_2C–(C_6H_4)–CO_2H$ (WAKO, 95%); 1,4-naphthalene dicarboxylic acid $HO_2C–(C_{10}H_8)–CO_2H$

16   (WAKO, 95%); imidazole (WAKO, 99%) and imidazole (D–4, CIL, 98%) were used as received.

17   Distilled water was used.

18   **Synthesis of $\{Al(\mu_2\text{-}OH)(1,4\text{-}ndc)\}_n$ (1)**

19   A mixture of $Al(NO_3)_3 \cdot 9H_2O$ (0.375 g, 1.0 mmol); 1,4-naphthalene dicarboxylic acid (0.108 g, 0.5

20   mmol) and deionized water (10 mL) was placed in a 23 mL Teflon autoclave and heated at 180 °C for

21   one day. The initial pH of the reaction mixture was 2.5 and the final pH was 2.0. After filtering and

22   washing the crude product with distilled water, a pure, light-yellow powder of $\mathbf{1} \cdot 2H_2O$ was obtained

23   (yield 80%). The sample was evacuated at 150 °C for 12 hours to afford the guest-free compound **1**.

24   **Synthesis of $\{Al(\mu_2\text{-}OH)(1,4\text{-}bdc)\}_n$ (2)**

1   The synthesis of **2** was carried out under hydrothermal conditions using Al(NO$_3$)$_3$·9H$_2$O (1.30 g, 3.5

2   mmol); 1,4-benzenedicarboxylic acid (0.288 g, 2.5 mmol) and distilled water (10 mL). The reaction was

3   performed in a 23 mL Teflon autoclave. The reaction mixture was heated at 220 °C for three days. After

4   filtering and washing with distilled water, a white powder was obtained. It was identified by powder

5   X-ray diffraction analysis. The excess terephthalic acid in the pores was removed by high-temperature

6   treatment at 330 °C for three days. X-ray powder diffraction (XRPD) analysis revealed that the material

7   was the guest-free compound **2**.

8   **Preparation of imidazole-loaded frameworks**

9   Products **1** and **2** were again degassed by heating to 120 °C under reduced pressure for 12 h to

10   remove guest molecules. Imidazole was vaporized into guest-free **1** and **2** at 120 °C, overnight, to yield

11   **1**⊃Imi and **2**⊃Imi. XRPD patterns of both these compounds confirmed that the frameworks were

12   maintained. The amount of loaded imidazole was determined by TG analysis.

13   **Proton conductivity measurement of 1⊃Im and 2⊃Im**

14   Samples for conductivity measurements were prepared by sandwiching the respective powders

15   **1**⊃Im and **2**⊃Im between two gold-coating electrodes (diameter 3 mm) and then tightly connecting the

16   two electrodes, by means of springs, to ensure good contact between the sample and each electrode.

17   Temperature-dependent conductivities of **1**⊃Im and **2**⊃Im were determined using alternative current

18   (AC) impedance spectroscopy (Solartron SI 1260 Impedance/Gain-Phase analyzer), using a homemade

19   cell over the frequency range 1 Hz – 10 MHz and with an input voltage amplitude of 100 mV. The

20   measurement cell was filled with nitrogen at atmospheric pressure prior to recording the measurements.

21   ZView software was utilized to extrapolate impedance data results via equivalent circuit simulation to

22   complete the Nyquist plot and obtain the resistance values.

23   **^{2}H solid-state NMR**

1   Solid-state ^{2}H NMR spectra were recorded using a Varian Chemagnetics CMX-300 spectrometer, at

2   45.826 MHz, and a quadrupole echo pulse sequence. Simulated spectra were produced with FORTRAN

3   programs written by us.
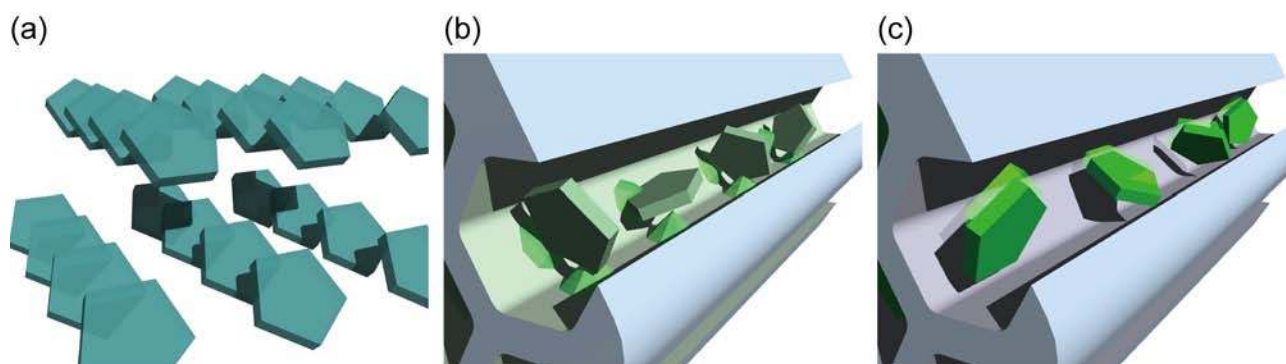
4

1   **FIGURE CAPTIONS**

2

Figure 1. Imidazole molecules are densely packed with low mobility that adversely affects proton transport process. This occurs in the bulk solid (a). Imidazole accommodated in nanochannel containing the active site with a high affinity to imidazole. The strong host−guest interaction retards the mobility of imidazole to afford the low proton conductivity (b). Imidazoles are accommodated in nanochannel without strong host−guest interaction, and therefore, the molecules obtain the high mobility to show high proton conductivity (c).

3
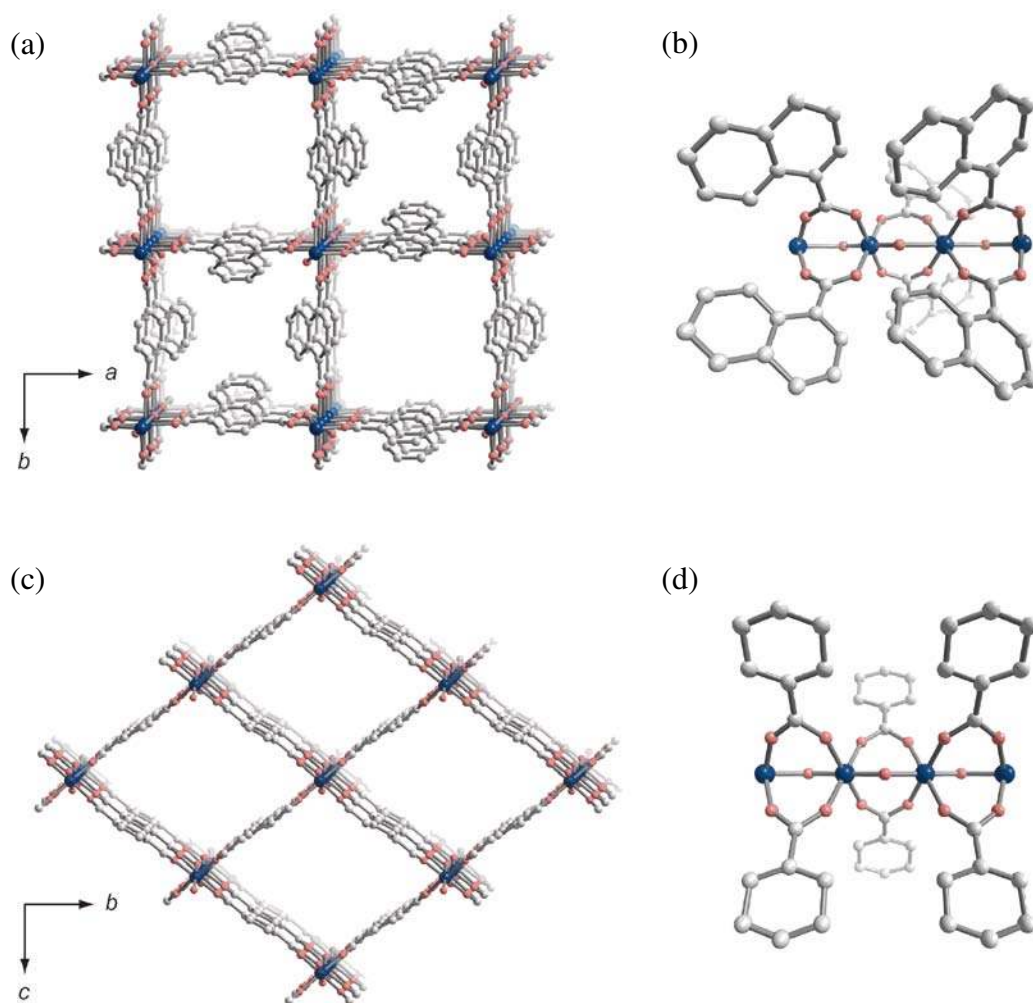
Figure 2. 3D structures of **1** (a) and **2** (c). Al, C, and O are represented in blue, gray, and red, respectively. H atoms are omitted for clarification. (b) and (d) show comparison of ligand size effect on μ_2-OH group of **1** and **2** respectively.
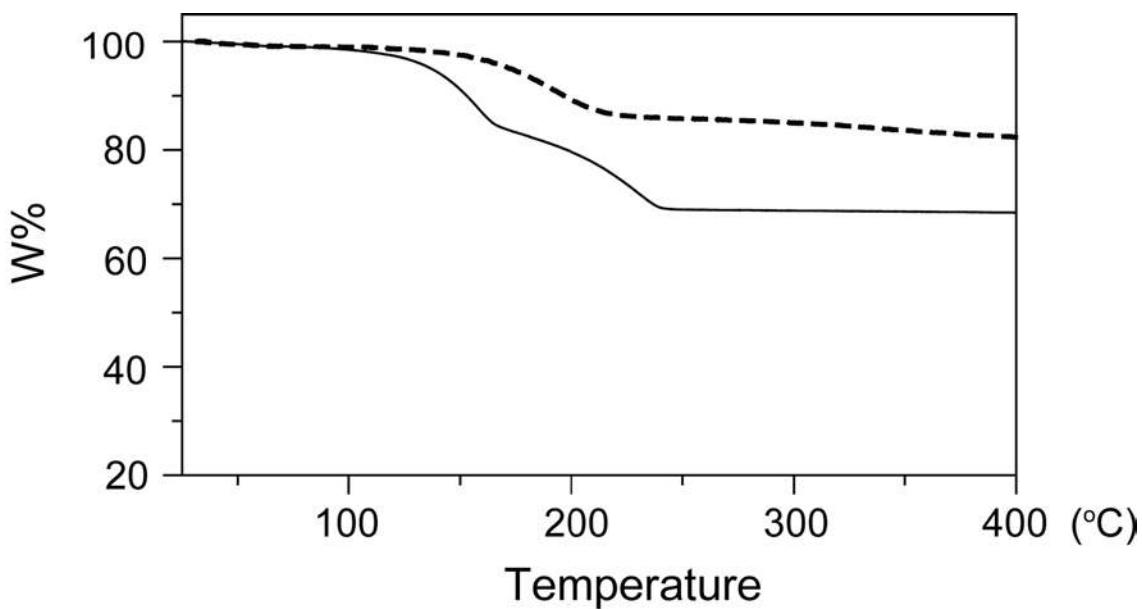
1

Figure 3. TGA curves for **1**⊃Im (dash line) and **2**⊃Im (solid line) over the temperature range from 25 – 400 $^{\circ}$C at heating rate 10 $^{\circ}$C min^{-1} under N_2 atmosphere. The guest release of **1**⊃Im occurs in one single step that clues the homogeneous installation of imidazole in **1**, whereas of **2**⊃Im occurs in two steps, indicating two types of imidazole (strongly and weakly interacts with **2**).
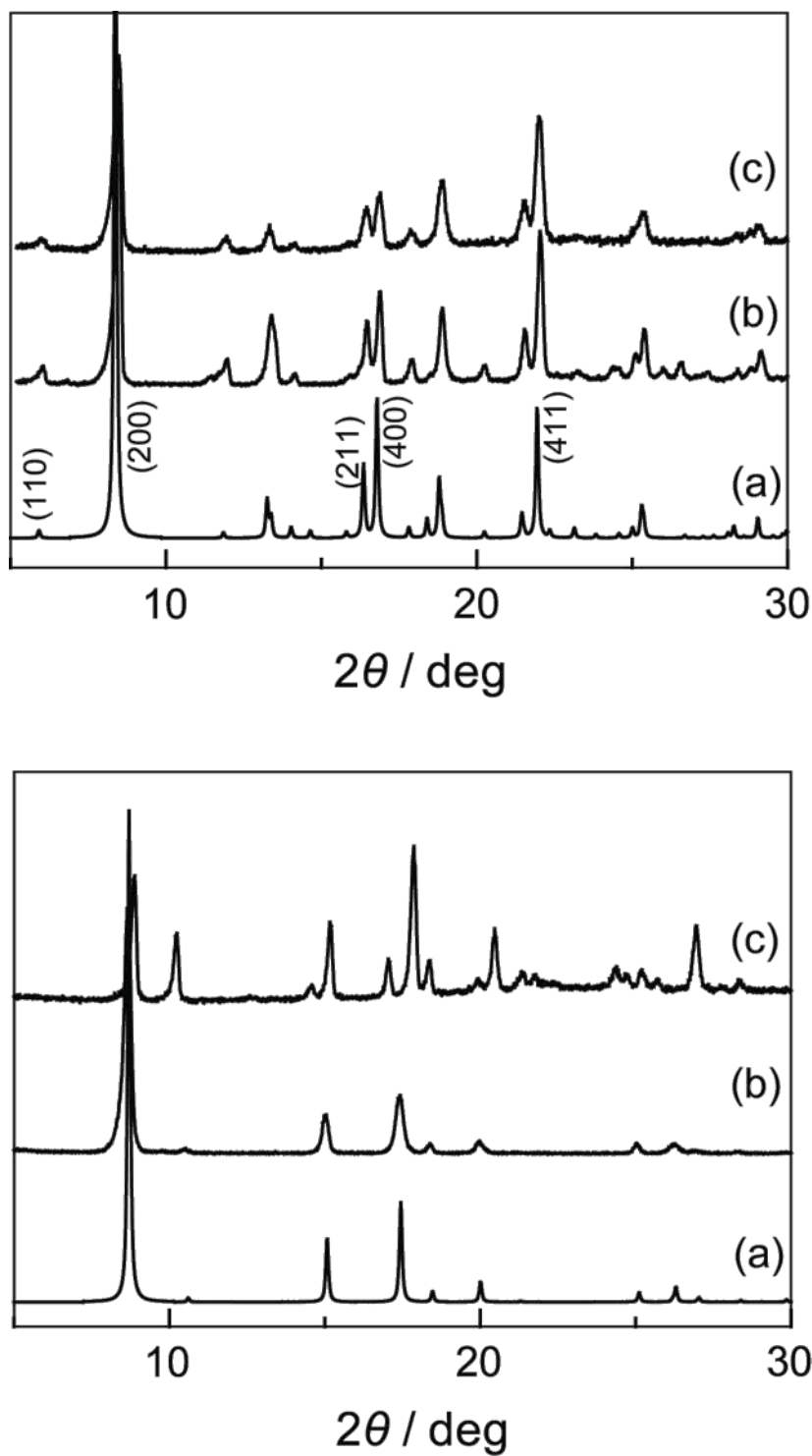
1

15

Figure 4. Above: XRPD patterns of simulated **1**·2H$_2$O (a), **1** (b), and **1**⊃Im (c). The patterns before and after accommodation of imidazole are identical. Below: XRPD patterns of simulated **2** (a), **2** (b), and **2**⊃Im (c). A change in XRPD patterns after accommodation of imidazole is observed.[39]
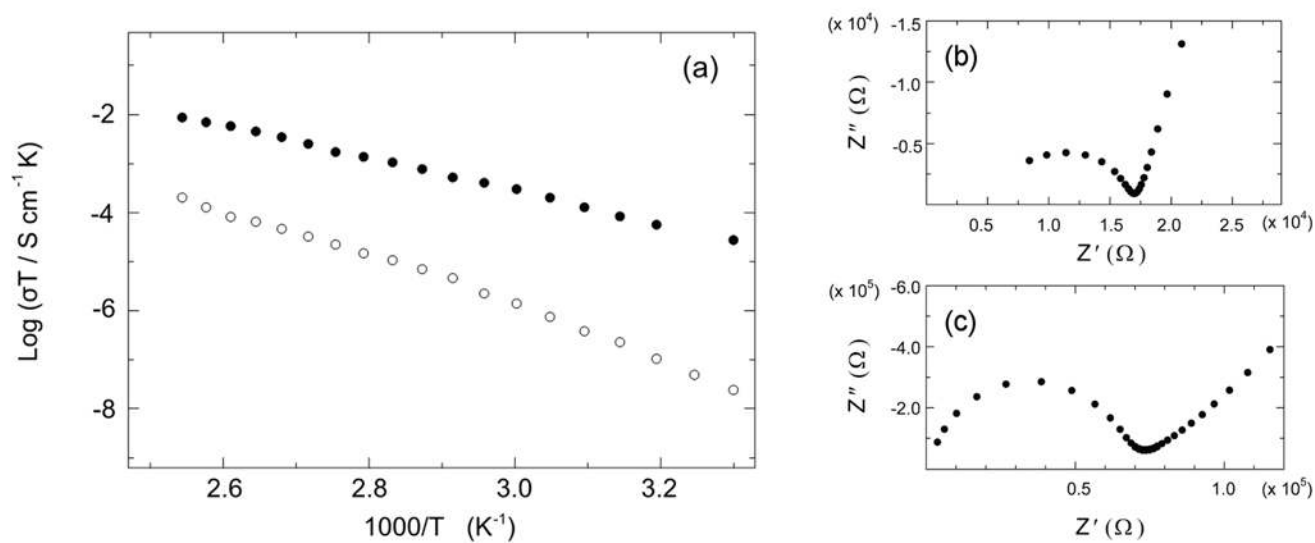
1

Figure 5. (a) Proton conductivity of **1**⊃Im (filled dots) and **2**⊃Im (empty dots) under anhydrous condition performed by A.C. impedance analyzer. Nyquist diagrams of **1**⊃Im (b) and **2**⊃Im (c) at
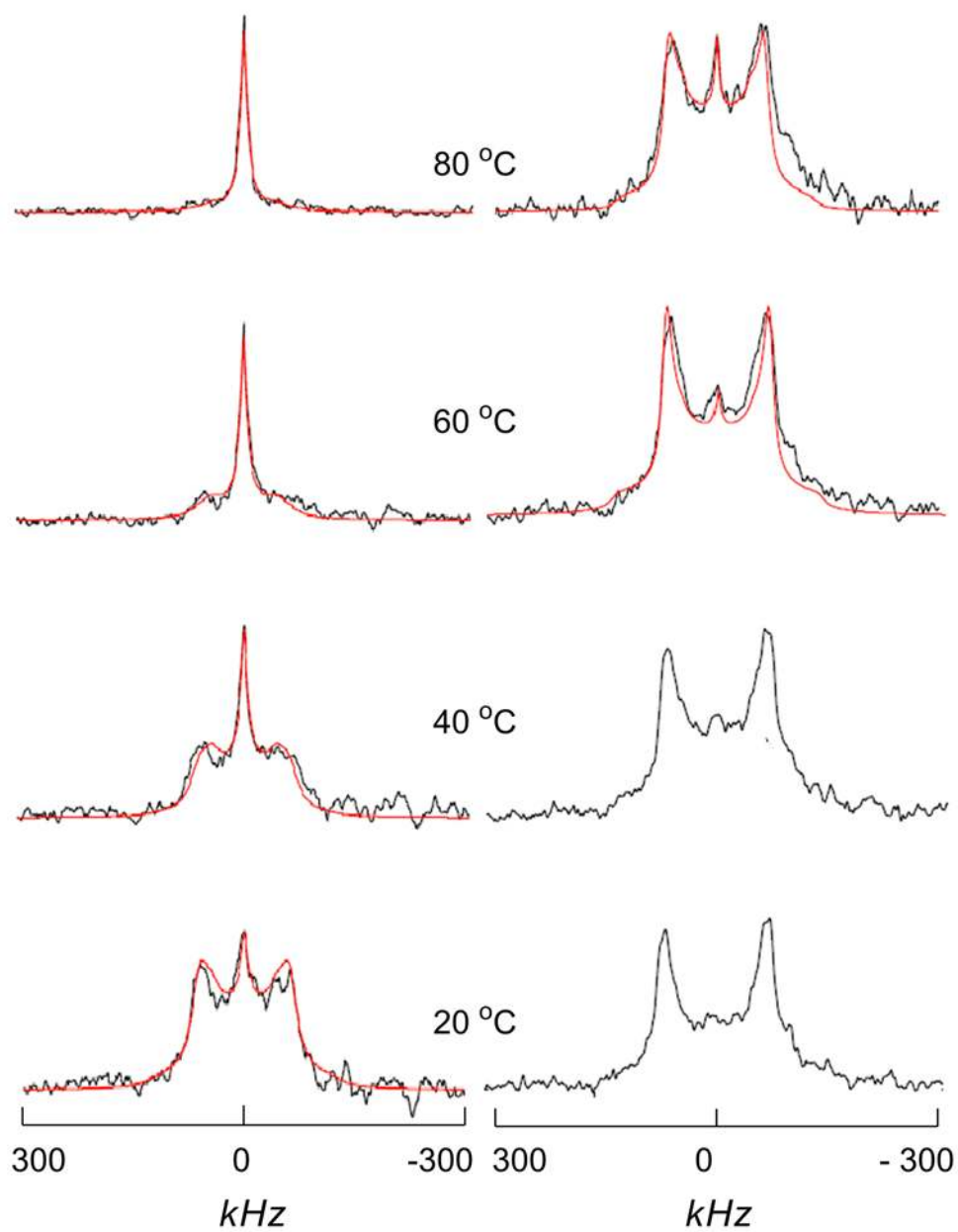
1
2

Figure 6. ^{2}H solid-state NMR spectra of **1**⊃Im-d_4 (left) and **2**⊃Im-d_4 (right). The simulation results

are shown in red lines.

1
2

References:

[1] Kreuer, K. D., Paddison, S. J., Spohr, E. and Schuster, M., Transport in Proton Conductors for Fuel-Cell Applications: Simulations, Elementary Reactions, and Phenomenology. *Chem. Rev.* **104** (10), 4637 (2004).

[2] Martin F.H. Schuster and Meyer, W. H., Anhydrous Proton-Conducting Polymers. *Annu. Rev. Mater. Res.* **33**, 233 (2003).

[3] Jannasch, P., Recent developments in high-temperature proton conducting polymer electrolyte membranes. *Curr. Opin. Colloid Interface Sci.* **8** (1), 96 (2003).

[4] Li, S.et al., Synthesis and properties of imidazole-grafted hybrid inorganic-organic polymer membranes. *Electrochim. Acta* **51** (7), 1351 (2006).

[5] West, A. R., *Basic Solid State Chemistry*. (Wiley, 1999).

[6] Kawada, A., McGhie, A. R. and Labes, M. M., Protonic Conductivity in Imidazole Single Crystal. *J. Chem. Phys.* **52** (6), 3121 (1970).

[7] Noro, S., Kitagawa, S., Kondo, M. and Seki, K., A New, Methane Adsorbent, Porous Coordination Polymer. *Angew. Chem. Int. Ed.* **39** (12), 2081 (2000).

[8] Rowsell, J. L. and Yaghi, O. M., Strategies for hydrogen storage in metal-organic frameworks. *Angew. Chem. Int. Ed.* **44** (30), 4670 (2005).

[9] Ferey, G.et al., Hydrogen adsorption in the nanoporous metal-benzenedicarboxylate $M(OH)(O_2C-C_6H_4-CO_2)(M = Al^{3+}, Cr^{3+})$, MIL-53. *Chem. Commun.* (24), 2976 (2003).

[10] Rosi, N. L.et al., Hydrogen Storage in Microporous Metal-Organic Frameworks. *Science* **300** (5622), 1127 (2003).

[11] Li, H., Eddaoudi, M., O'Keeffe, M. and Yaghi, O. M., Design and synthesis of an exceptionally stable and highly porous metal-organic framework. *Nature* **402** (6759), 276 (1999).

[12] Cychosz, K. A., Wong-Foy, A. G. and Matzger, A. J., Liquid Phase Adsorption by Microporous Coordination Polymers: Removal of Organosulfur Compounds. *J. Am. Chem. Soc.* **130** (22), 6938 (2008).

[13] Finsy, V.et al., Pore-Filling-Dependent Selectivity Effects in the Vapor-Phase Separation of Xylene Isomers on the Metal-Organic Framework MIL-47. *J. Am. Chem. Soc.* **130** (22), 7110 (2008).

[14] Bradshaw, D.et al., Permanent Microporosity and Enantioselective Sorption in a Chiral Open Framework. *J. Am. Chem. Soc.* **126** (19), 6106 (2004).

[15] Dybtsev, D. N.et al., Microporous Manganese Formate: A Simple Metal-Organic Porous Material with High Framework Stability and Highly Selective Gas Sorption Properties. *J. Am. Chem. Soc.* **126** (1), 32 (2004).

16   Min, K. S. and Suh, M. P., Self-Assembly and Selective Guest Binding of Three-Dimensional Open-Framework Solids from a Macrocyclic Complex as a Trifunctional Metal Building Block. *Chem. Eur. J.* **7** (1), 303 (2001).

17   Wang, B.et al., Colossal cages in zeolitic imidazolate frameworks as selective carbon dioxide reservoirs. *Nature* **453** (7192), 207 (2008).

18   Hasegawa, S.et al., Three-Dimensional Porous Coordination Polymer Functionalized with Amide Groups Based on Tridentate Ligand: Selective Sorption and Catalysis. *J. Am. Chem. Soc.* **129** (9), 2607 (2007).

19   Horike, S., Dinca, M., Tamaki, K. and Long, J. R., Size-Selective Lewis Acid Catalysis in a Microporous Metal-Organic Framework with Exposed Mn^{2+} Coordination Sites. *J. Am. Chem. Soc.* **130** (18), 5854 (2008).

20   Cho, S.-H.et al., A metal-organic framework material that functions as an enantioselective catalyst for olefin epoxidation. *Chem. Commun.* (24), 2563 (2006).

21   Horcajada, P.et al., Synthesis and catalytic properties of MIL-100(Fe), an iron(III) carboxylate with large pores. *Chem. Commun.* (27), 2820 (2007).

22   Schroder, F.et al., Ruthenium Nanoparticles inside Porous [Zn4O(bdc)3] by Hydrogenolysis of Adsorbed [Ru(cod)(cot)]: A Solid-State Reference System for Surfactant-Stabilized Ruthenium Colloids. *J. Am. Chem. Soc.* **130** (19), 6119 (2008).

23   Ingleson, M. J.et al., Generation of a solid Bronsted acid site in a chiral framework. *Chem. Commun.* (11), 1287 (2008).

24   Fujita, M., Kwon, Y. J., Washizu, S. and Ogura, K., Preparation, Clathration Ability, and Catalysis of a Two-Dimensional Square Network Material Composed of Cadmium(II) and 4,4'-Bipyridine. *J. Am. Chem. Soc.* **116** (3), 1151 (1994).

25   Seo, J. S.et al., A homochiral metal-organic porous material for enantioselective separation and catalysis. *Nature* **404** (6781), 982 (2000).

26   Evans, O. R., Ngo, H. L. and Lin, W., Chiral Porous Solids Based on Lamellar Lanthanide Phosphonates. *J. Am. Chem. Soc.* **123** (42), 10395 (2001).

27   Ferey, G.et al., Mixed-Valence Li/Fe-Based Metal-Organic Frameworks with Both Reversible Redox and Sorption Properties. *Angew. Chem. Int. Ed.* **46** (18), 3259 (2007).

28   Kitagawa, H.et al., Highly proton-conductive copper coordination polymer, H2dtoaCu (H2dtoa=dithiooxamide anion) *Inorg. Chem. Commun.* **6** (4), 346 (2003).

29   Yamada, T., Sadakiyo, M. and Kitagawa, H., High Proton Conductivity of One-Dimensional Ferrous Oxalate Dihydrate. *J. Am. Chem. Soc.* **131** (9), 3144 (2009).

30 Uemura, T.et al., Radical polymerisation of styrene in porous coordination polymers. *Chem. Commun.* (48), 5968 (2005).

31 Uemura, T.et al., Conformation and Molecular Dynamics of Single Polystyrene Chain Confined in Coordination Nanospace. *J. Am. Chem. Soc.* **130** (21), 6781 (2008).

32 Mulfort, K. L. and Hupp, J. T., Chemical Reduction of Metal-Organic Framework Materials as a Method to Enhance Gas Uptake and Binding. *J. Am. Chem. Soc.* **129** (31), 9604 (2007).

33 Muller, M.et al., Loading of MOF-5 with Cu and ZnO nanoparticles by gas-phase infiltration with organometallic precursors: Properties of Cu/ZnO@MOF-5 as catalyst for methanol synthesis. *Chem. Mater.* **20** (14), 4576 (2008).

34 Turner, S.et al., Direct Imaging of Loaded Metal-Organic Framework Materials (Metal@MOF-5). *Chem. Mater.* **20** (17), 5622 (2008).

35 Horcajada, P.et al., Flexible Porous Metal-Organic Frameworks for a Controlled Drug Delivery. *J. Am. Chem. Soc.* **130** (21), 6774 (2008).

36 Horcajada, P.et al., Metal-Organic Frameworks as Efficient Materials for Drug Delivery. *Angew. Chem. Int. Ed.* **45** (36), 5974 (2006).

37 Tanaka, D.et al., Anthracene array-type porous coordination polymer with host-guest charge transfer interactions in excited states. *Chem. Commun.* (30), 3142 (2007).

38 Comotti, A.et al., Nanochannels of Two Distinct Cross-Sections in a Porous Al-Based Coordination Polymer. *J. Am. Chem. Soc.* (2008).

39 Loiseau, T.et al., A Rationale for the Large Breathing of the Porous Aluminum Terephthalate (MIL-53) Upon Hydration. *Chem. Eur. J.* **10** (6), 1373 (2004).

40 Serre, C.et al., An Explanation for the Very Large Breathing Effect of a Metal-Organic Framework during CO2 Adsorption. *Adv. Mater.* **19** (17), 2246 (2007).

41 Spek, A. L., Foundations of Crystallography. *Acta Crystallogr., Sect. A* **A46**, c34 (1990).

42 Craven, B. M., McMullan, R. K., Bell, J. D. and Freeman, H. C., The crystal structure of imidazole by neutron diffraction at 20 oCand -150 oC. *Acta Crystallogr., Sect. B* **33** (8), 2585 (1977).

43 Horike, S.et al., Motion of methanol adsorbed in porous coordination polymer with paramagnetic metal ions. *Chem. Commun.* (19), 2152 (2004).

44 Ueda, T.et al., Phase transition and molecular motion of cyclohexane confined in metal-organic framework, IRMOF-1, as studied by 2H NMR. *Chem. Phys. Lett.* **443** (4-6), 293 (2007).

45 Horike, S.et al., Dynamic Motion of Building Blocks in Porous Coordination Polymers13. *Angew. Chem. Int. Ed.* **45** (43), 7226 (2006).

[46] Schmidt-Rohr, K. and Spiess, H. W., *Multidimensional Solid-State NMR and Polymers*. (Academic Press, London, 1994).

[47] Abragam, A., *Principles of Nuclear Magnetism* (Oxford University Press, Oxford, 1961).

[48] Bozkurt, A. and Meyer, W. H., Proton conducting blends of poly(4-vinylimidazole) with phosphoricacid. *Solid State Ionics* **138**, 259 (2001).